A Density Functional and Thermochemical Study of M−X Bond Lengths and Energies in $[MX_6]^{2-}$ Complexes: LDA versus Becke88/Perdew86 Gradient-Corrected Functionals

Robert J. Deeth* and H. Donald Brooke Jenkins

Inorganic Computational Chemistry Group, Department of Chemistry, University of Warwick, Coventry CV4 7AL, U.K.

Received: January 30, 1997; In Final Form: April 21, 1997[⊗]

Local density approximation (LDA) and Becke88/Perdew86 gradient-corrected density functional theory calculations are used to estimate the heterolytic bond energy, E(M−X), corresponding to the process $[MX_6]_g^{2-} \rightarrow M_g^{4+} + 6X_g^-$. The computed data, including scalar relativistic corrections for second- and third-row metals, are benchmarked against updated values for the bonds Zr−Cl, Mo−Cl, Pd−Cl, Sn−Cl, Hf−Cl, W−Cl, W−Br, Re−Cl, Re−Br, Os−Cl, Ir−Cl, Pt−Cl, Pt−Br, Ti−Cl, Ti−Br, and Ni−F derived from a combination of thermochemical and computational data on the antifluorite A_2MX_6 hexahalometallate(IV) salts. The LDA tends to overbind, and the bond energies are generally too large. The BP method systematically reduces these values by about 60 kJ mol^{-1}, giving a significantly better comparison with experiment. However, LDA-optimized M−X bond lengths, both *in vacuo* and for a model 'in crystal' $\{K_8[PdCl_6]\}^{6+}$ cluster, are generally in better agreement with experiment.

Introduction

The local density approximation (LDA) in density functional theory (DFT) has found widespread application in transition metal chemistry[1] and is known to give a better description of metal−ligand bonding than conventional molecular orbital (MO) approaches based on single-determinant Hartree−Fock theory.[1a,2] However, the LDA formally refers to a uniform, or at least slowly varying, electron density and tends to overemphasize chemical binding.[3] Empirical[4] or more stringent scaling modifications[5] of the LDA can be made in the form of "gradient corrected" (GC) functionals, which attempt to model more realistically the density gradients in molecules. Where experimental data exist for comparison, these GC methods give improved bond energies compared to those from LDA approaches. For organometallic species, for example, this improvement in binding energies is also accompanied by more accurate GC-optimized structures. In contrast, for Werner-type TM complexes, we have shown[3b] that the LDA gives better metal−ligand distances than those from a GC scheme.[4]

At that time, we had no experimental measures of bond energies and so could only speculate whether the better performance of the LDA for M−L distances in Werner complexes would also imply better LDA M−L binding energies. If true, such a result has significant implications for the design of new functionals which would need to retain the essence of the LDA in order to handle Werner complexes but still incorporate those features which improve the treatment of other classes of molecule. On the other hand, if GC functionals give better binding energies for Werner complexes too, there remains the question of why the geometries are apparently less accurate. The challenge for new functionals would then be, presumably, to retain only those aspects of the LDA which affect the geometry and then modify the rest to improve the binding energies. Either way, it seems that an even more fundamental understanding of the basic LDA is required.

Analysis of these issues requires experimental estimates of M−L binding energies to gauge the performance of a given functional. The net charge on many Werner complexes leads to large environmental effects in solution and the solid state, and it is difficult to make direct thermochemical measurements on the isolated complexes themselves. However, there is a combined experimental/computational approach, originally developed by Jenkins and Pratt,[7] which uses thermochemical considerations and total lattice potential energy calculations[8] to derive heterolytic bond energies E(M−X).[9] For antifluorite compounds of general formula A_2MX_6, a range of octahedral M(IV) centers have been treated.[6] These 'experimental' results provide an ideal test bed for evaluating the relative performance of LDA and GC methods. Doubly so since they formally refer to a hypothetical *in vacuo* $[MX_6]^{2-}$ species with the M−X distance relevant to the solid state structure but otherwise free from crystal environment effects. The derived bond energies can, for the first time, be compared directly to the DFT *in vacuo* results for discrete Werner-type complexes and complement our previous study on M−L distances.

Thermochemical Methods and Molecules Studied

The thermochemical bond energies E(M−X) in octahedral ions $[MX_6]^{2-}$ are normally defined with reference to the heterolytic fission of the bond according to eq 1.

$$[MX_6]_g^{2-} \rightarrow M_g^{4+} + 6X_g^- \tag{1}$$

The definition

$$E(\mathrm{M-X}) = -1/6\Delta_f H^i([MX_6]^{2-},g) \tag{2}$$

has long been adpoted[10] because common substitution reactions in inorganic coordination chemistry usually involve heterolytic rather than homolytic fission of the M−X bonds and the ionic nature of metal−halogen bonds makes it natural to think of complexes as dissociating into ions. Such bond energies can be derived from the thermochemical cycle shown in Figure 1 using eq 3:

$$E(\mathrm{M-X}) = {}^1/_6[2\Delta_f H^o(A^+,g) + \Delta_f H^o(M^{4+},g) + 6\Delta_f H^o(X^-,g) - \Delta_f H^o(A_2MX_6,c) - U_{POT}(A_2MX_6) + {}^3/_2RT] \tag{3}$$

[⊗] Abstract published in *Advance ACS Abstracts,* June 1, 1997.

S1089-5639(97)00374-5 CCC: $14.00 © 1997 American Chemical Society

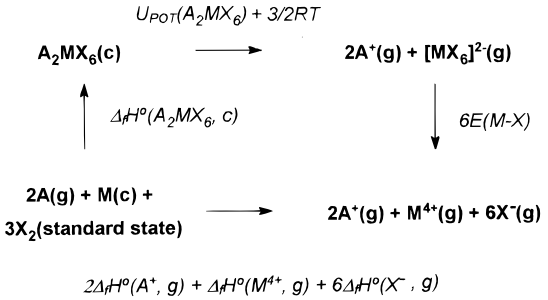

Figure 1. Thermodynamic scheme for evaluating heterolytic bond energies.

where U_{POT} is the total lattice potential energy of the hexahalometallate(IV) salt A_2MX_6. To relate this to the lattice enthalpy ΔH_L, we first consider the relationship between U_{POT} and ΔE, the sum of the total absolute internal energies of A^+, $[MX_6]^{2-}$, and A_2MX_6 (eq 4 and Figure 2):[11]

$$\Delta E = 2E(A^+) + E([MX_6]^{2-}) - E(A_2MX_6) \quad (4)$$

U_{ACOU} is the acoustic potential of the crystal lattice and is related to U_{POT} *via* eq 5 (see also Figure 2).

$$U_{POT} = U_{TOTAL} + U_{ACOU} \quad (5)$$

It is reasonable to assume that the degrees of internal vibrational freedom of the $[MX_6]^{2-}$ anions are equally excited in the crystal and in the hypothetical gas at the same temperature and can be neglected. However, the rotational degrees of freedom must be included with the result that

$$\Delta E = {}^9/_2RT + U_{TOTAL} \quad (6)$$

$$\Delta E = {}^9/_2RT + U_{POT} - U_{ACOU} \quad (7)$$

U_{ACOU} can be calculated from the temperature variation of heat capacities and the lattice zero point energy or by the Einstein or Debye theories of heat capacities. When the temperature is much larger than the Einstein, Θ_E, or the Debye, Θ_D, characteristic temperatures

$$U_{ACOU} = 9RT \quad (8)$$

and the lattice enthalpy ΔH_L is given by

$$\Delta H_L = \Delta E + \Delta nRT \quad (9)$$

$$\Delta H_L = U_{POT} - {}^3/_2RT \quad (10)$$

For the purposes of calculation,

$$\Delta_f H^o(M^{4+},g) = \sum_{i=1}^{4} I_i + \Delta_f H^o(M,g) \quad (11)$$

where I_i represents the ionization potential of the process

$$M_g^{i-1+} - e \rightarrow M_g^{i+} \quad (12)$$

Bond energies derived from the thermochemistry of a series of hexahalometallate(IV) complexes possessing the antifluorite crystal lattice structure have been obtained using the data in Table 1 and ref 6. Table 1 also lists values of $\Delta_f H^i([MX_6]^{2-},g)$ corresponding to the reverse of process 1.

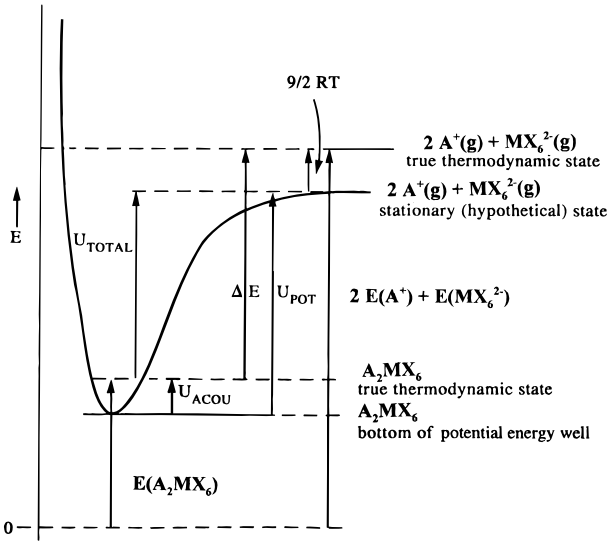

Figure 2. Relationship between the total lattice potential energy of A_2MX_6, $U_{POT}(A_2MX_6)$, and the internal energy change ΔE for the process $A_2MX_6(c) \rightarrow 2A^+(g) + [MX_6]^{2-}(g)$, giving rise to eqs 4−6.

Computational Details: DFT

The DFT calculations reported here are based on the Kohn−Sham formalism[14] as implemented in the Amsterdam density functional (ADF) program suite version 2.0.1.[15] LDA results used the correlation functional parameterized by Vosko, Wilk, and Nusair.[16] Additionally, gradient corrections employed the formulations of Becke for exchange[4a] and Perdew for correlation.[4b] Triple-ζ STO expansions for the valence orbitals were employed with an additional p function for the metals (ADF basis set IV) and additional d and f functions on the halides (ADF basis set V). All geometries were optimized using analytical energy gradients[17] under the constraint of O_h symmetry. Low-spin electronic configurations were assumed for all complexes. Calculations were performed spin unrestricted where appropriate with scalar relativistic corrections[18] for all second- and third-row metal species. The reference state for binding energies was generated relative to an isolated, spin unrestricted M^{4+} cation and six closed shell halide anions. Zero-point energies and temperature corrections to the enthalpy were computed for selected complexes at the LDA-optimized geometry assuming ideal gas behavior and the expressions from standard statistical thermodynamics. Default ADF 2.0.1 convergence criteria were used for the self-consistent field and geometry optimization procedures.

Results and Discussion

The computed and observed heterolytic bond enthalpies are collected in Table 2. The DFT values have been corrected to ΔH_{298} values by computing zero-point energies and the temperature dependence of the enthalpy as described above. Any variation between these correction terms arises from the vibrational contribution to the relevant partition functions. For the complexes studied, the computed vibrational spectra depend, to a good approximation, only on the nature of the halide. The total correction (zero-point energy plus temperature correction to ΔH) is about 90, 65, and 60 kJ mol^{-1} for F^-, Cl^-, and Br^- complexes, respectively, which, per bond, only amounts to a 15, 11, and 10 kJ mol^{-1} change, *i.e.*, about 1% or less of the heterolytic bond enthalpy.

TABLE 1: Thermochemical Data, Total Lattice Potential Energies and Derived $\Delta_f H^i([MX_6]^{2-},g)$ and Heterolytic Bond Enthalpies E(M−X). All Numerical Data in kJ mol^{-1}

bond	compound	$\Delta_f H^o(M^{4+},g)$	$\Delta_f H^o(A_2MX_6,c)$	$U_{POT}(A_2MX_6)$	$\Delta_f H^i([MX_6]^{2-},g)$	E(M−X)
Ni−F	K_2NiF_6	11896[7a]	−2021 ± 12[13a]	1721[7b]	−11694	1949
Zr−Cl	K_2ZrCl_6	8047.2[13b−c]	−1932 ± 4[13f]	1339[7b]	−8268	1378
Zr−Cl	Cs_2ZrCl_6	8047.2[13b−c]	−1992 ± 4[13f]	1348[7b]	−8208	1368
Mo−Cl	Na_2MoCl_6	9996.2[1b]	−1376[13f]	1526[7b]	−9660	1610
			1372[13f]	1530[7b]		
Mo−Cl	K_2MoCl_6	9996.2[13b−e]	−1475[13f]	1418[7b]	−9678	1613
			−1465[13h]			
			−1469[13f]			
			−1466.1[12a]			
Mo−Cl	Rb_2MoCl_6	9996.2[13b−e]	−1479[13h]	1399[7b]	−9672	1612
			−1495[13f]	1383[7b]		
Mo−Cl	Cs_2MoCl_6	9996.2[13b−e]	−1527[13f]	1347[7b]	−9696	1616
			−1512[13h]	1332[7b]		
Pd−Cl	K_2PdCl_6	11064[7b]	−1187[13i]	1481[7b]	−10434	1739
			−1226.3[12a]	1450[7b]		
Sn−Cl	K_2SnCl_6	9320.7[12a]	−1477.0[12a]	1352[7b]	−9078	1513
			−1518[13i]	1363[7b]		
			−1485[13j]			
			−1481.7[13k]			
Sn−Cl	Rb_2SnCl_6	9320.7[12a]	−1529[131]	1358[7b]	−9072	1512
			−1523.0[12a]	1361[7b]		
Hf−Cl	K_2HfCl_6	8192[12a]	−1957 ± 12[131]	1345[7b]	−8328	1388
			−1966[12a]	1571[7b]		
W−Cl	K_2WCl_6	9155[7b]	−1380[13m]	1398[7b]	−8754	1459
			−1359[13g,n]			
W−Cl	Rb_2WCl_6	9155[7b]	−1429[13g,n]	1397[7b]	−8766	1461
W−Cl	Cs_2WCl_6	9155[7b]	−1446[13g,n]	1392[7b]	−8724	1454
W−Br	K_2WBr_6	9155[7b]	−1106[13m]	1361[7b]	−8568	1428
W−Br	Cs_2WBr_6	9155[7b]	−1132[13m]	1362[7b]	−8526	1421
Re−Cl	K_2ReCl_6	9460[7b]	−1333[13o]	1501[13q]	−8952	1492
			−1331[13p]	1476[13q]		
			−1310.4[12a]	1416[7b]		
				1458[13q]		
Re−Br	K_2ReBr_6	9460[7b]	−1036[13m]	1445[13q]	−8766	1461
				1404[13q]	−8808	1468
				1375[7b]	−8622	1437
Os−Cl	K_2OsCl_6	9700[7b]	−1171[13i]	1447[7b]	−9066	1511
			−1197.5[12a]			
Ir−Cl	K_2IrCl_6	9558[7b]	−1197[13i]	1442[7b]	−8910	1485
			−1176[13r]			
			−1130[12a]			
Pt−Cl	K_2PtCl_6	10151[7b]	−1235[13r]	1468[7b]	−9306	1551
			−1229.3[12a]	1521[13r]		
Pt−Cl	Rb_2PtCl_6	10151[7b]	−1251[13r]	1464[7b]	−9306	1551
			−1246[12a]			
Pt−Cl	Ag_2PtCl_6	10151[7b]	−527[13t]	1773[7b]	−9336	1556
Pt−Br	K_2PtBr_6	10151[7b]	−1040[13i]	1423[7b]	−9270	1545
			−1021.3[12a]		−9252	1542
Ti−Cl	K_2TiCl_6	9288.5[12a]	−1747[13u]	1412[7b]	−9264	1544
			−1761[12a]			
Ti−Cl	Rb_2TiCl_6	9288.5[12a]	−1767[13u]	1415[7b]	−9228	1538
			−1778.2[12a]			
Ti−Cl	Cs_2TiCl_6	9288.5[12a]	−1797[13u]	1402[7b]	−9210	1535
			−1810[12a]			
Ti−Br	K_2TiBr_6	9288.5[12a]	−1493[13u]	1379 ± 32[7b]	−9114	1519
Ti−Br	Rb_2TiBr_6	9288.5[12a]	−1505[12a]	1341[7b]	−9162	1527
			−1517.0[13u]			
			−1612.0[13k,w]			
Ti−Br	Cs_2TiBr_6	9288.5[12a]	−1553[13u]	1339[7b]	−9150	1525
			−1543.9[12a]			
			−1644[13j,k]			
			−1641[13j]			

It is far more important to account for the relative energies of the free M^{4+} ions, particularly with regard to the number of unpaired electrons and the resulting energy lowering of a spin-unrestricted calculation. For example, the energy of a spin unrestricted d^5 Ir^{4+} ion at the relativistically corrected LDA level is 426 kJ mol^{-1} lower than the equivalent spin restricted case. The difference is about 60 kJ mol^{-1} greater when BP gradient corrections are included. The magnitude of the effect decreases fairly rapidly with the number of unpaired electrons falling from its peak of 426 kJ mol^{-1} at Ir^{4+} (five unpaired electrons) to 277, 159, and 72 kJ mol^{-1} for Os^{4+}, Re^{4+}, and W^{4+} with four, three, and two unpaired electrons, respectively. The energy changes also depend quite strongly on the atomic number. For example, for the d^6 ions Ni^{4+}, Pd^{4+}, and Pt^{4+}, spin polarization lowers the calculated (LDA) energy by 468, 296, and 267 kJ mol^{-1}, respectively.

Having corrected the calculated M−X bond energies, the differences between theory and experiment are shown in Figure 3. The Becke88/Perdew86 (BP) gradient corrections uniformly reduce the LDA bond energies by about 4%, and with only two

TABLE 2: M−X Heterolytic Bond Energies Calculated Using LDA and BP Functionals Compared with the Thermochemical Estimates (kJ mol^{-1})

	heterolytic bond energies[a]		
complex	LDA	BP	av thermochemical data[b]
$[TiCl_6]^{2-}$	1610	1558	1539
$[TiBr_6]^{2-}$	1620	1524	1524
$[NiF_6]^{2-}$	2034	1968	1949
$[ZrCl_6]^{2-}$	1401	1348	1373
$[MoCl_6]^{2-}$	1553	1492	1613
$[PdCl_6]^{2-}$	1789	1721	1739
$[SnCl_6]^{2-}$	1545	1487	1513
$[HfCl_6]^{2-}$	1397	1353	1388
$[WCl_6]^{2-}$	1522	1459	1458
$[ReCl_6]^{2-}$	1570	1503	1492
$[OsCl_6]^{2-}$	1608	1539	1511
$[IrCl_6]^{2-}$	1634	1568	1485
$[PtCl_6]^{2-}$	1709	1638	1554
$[WBr_6]^{2-}$	1494	1436	1425
$[ReBr_6]^{2-}$	1543	1380	1467
$[PtBr_6]^{2-}$	1692	1626	1544

[a] The calculated data include zero-point and finite temperature corrections. Scalar relativistic corrections are also included for second- and third-row metals. [b] The thermochemical estimates are averages of the data in Table 1.

TABLE 3: Calculated and Observed M−X Bond Lengths (Å)

	M−X Bond Lengths			
complex	LDA[a]	BP[a]	av obs ± spread[b]	*N*(obs)
$[TiCl_6]^{2-}$	2.35	2.40	2.35 ± 0.02	4
$[TiBr_6]^{2-}$	2.51	2.58	2.62 ± 0.02	2
$[NiF_6]^{2-}$	1.81	1.86	1.75 ± 0.03	2
$[ZrCl_6]^{2-}$	2.47	2.51	2.45 ± 0.01	2
$[MoCl_6]^{2-}$	2.37	2.41	2.30	1
$[PdCl_6]^{2-}$	2.32	2.38	2.30	1
$[SnCl_6]^{2-}$	2.47	2.52	2.42 ± 0.03	9
$[HFCl_6]^{2-}$	2.51	2.55	2.60	1
$[WCl_6]^{2-}$	2.41	2.46	2.36 ± 0.00	3
$[ReCl_6]^{2-}$	2.39	2.43	2.35	1
$[OsCl_6]^{2-}$	2.36	2.42	2.36	1
$[IrCl_6]^{2-}$	2.36	2.41	2.47	1
$[PtCl_6]^{2-}$	2.36	2.42	2.34 ± 0.04	5
$[WBr_6]^{2-}$	2.56	2.62	2.48 ± 0.00	2
$[ReBr_6]^{2-}$	2.53	2.60	2.48	1
$[PtBr_6]^{2-}$	2.50	2.58	2.46	1

[a] Calculated distances include scalar relativistic corrections for second- and third-row metal complexes. [b] Observed values are averages over *N*(obs) from Table III of ref 7a.

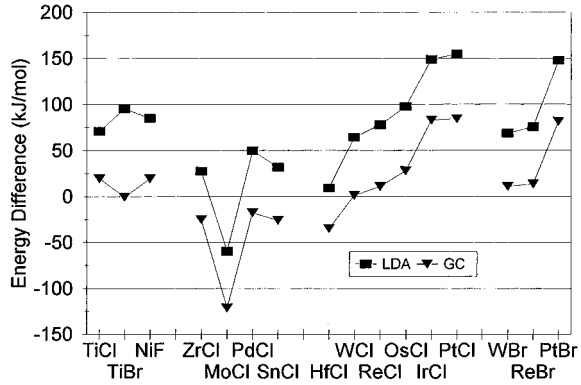

Figure 3. Differences between calculated (LDA and BP) and thermochemical bond energies, E(M−X) (kJ mol^{-1}).

exceptions, $[MoCl_6]^{2-}$ and $[HfCl_6]^{2-}$, the BP values are in better agreement with thermochemistry. Since the LDA estimates are almost always too high and since GC functionals are designed to reduce overbinding and will therefore lead to smaller

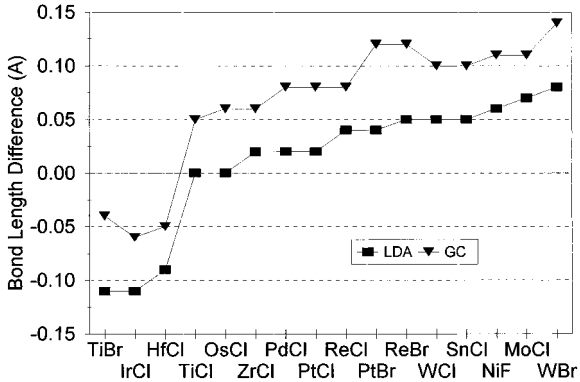

Figure 4. Differences between calculated (LDA and BP) and observed M−X bond lengths (Å).

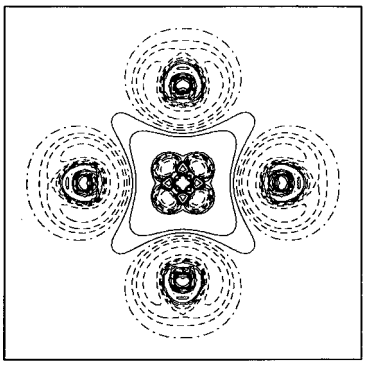

Figure 5. Calculated difference between total electron densities (LDA-BP) in the *xy* plane of $[PdCl_6]^{2-}$. Solid contours represent positive values, dashed contours negative values, and the dot−dash contour is zero. The lowest contour level is ±0.000 23. Successive contours differ by a factor of 2.

estimates of the bond energies, we can conclude that all GC functionals should be superior to the LDA. However, as found before, the LDA-optimized M−X distances generally agree better with experiment (Table 3 and Figure 4). Here there are three exceptions—$[TiBr_6]^{2-}$, $[IrCl_6]^{2-}$ and, once again, $[HfCl_6]^{2-}$—although the reason for this behavior is not especially obvious. At this point, therefore, we would conclude that while LDA calculations usually give better geometrical structures, binding energies are best computed using some form of GC DFT. The latter result is thus in keeping with the general performance of GC DFT for other types of chemical system.[1]

Thus, we are left with the intriguing question of why LDA geometries are apparently better when, intuitively, one would imagine that better energies (here BP ones) should also be accompanied by superior structural data. As discussed previously,[3b] the experimental structures are determined relative to a crystalline environment while the calculations formally refer to a vacuum. In order to establish an upper limit on the effect of the surrounding crystal on the optimized M−X distance, DFT calculations were performed on a $\{K_8[PdCl_6]\}^{6+}$ cluster. The K^+ ions were fixed at the corners of a cube with an edge length of 4.87 Å, being half the unit cell dimension determined for K_2PdCl_6. The crystalline environment has a minimal influence. The LDA-optimized Pd−Cl distance did not change significantly relative to the *in vacuo* distance of 2.32 Å, and there was only a 0.01 Å contraction at the BP level. In any event, the total calculated binding energy is a fairly weak function of the M−X distance such that any discrepancy in the bond length is not enough to alter the bond energy significantly. For example, changing the M−X distance by up to 0.08 Å only alters the total binding energy by 15−20 kJ mol^{-1}, which translates to about 3 kJ mol^{-1} for the heterolytic bond energy. Clearly,

TABLE 4: Extended Transition State Calculations for $[PdCl_6]^{2-}$ Relative to Pd^{4+} and Six Cl^{-a}

	Pauli	electrostatic	total steric	a_{1g}	e_g	t_{2g}	t_{1u}	total orbital	total binding
DDA	2948	−9405	−6457	−239	−992	−2890	−410	−4640	−11097
BP	3174	−9369	−6195	−227	−972	−2848	−387	−4540	−10735
Diff.	226	36	262	12	20	42	23	100	362

[a] Scalar relativistic corrections included. Only important components of orbital interactions included. All values in kJ mol^{-1}.

altering the bond lengths cannot compete with gradient corrections, the latter reducing the individual bond energy by about 60 kJ mol^{-1}.

To examine the relative behavior of LDA and BP functionals further, calculations for $[PdCl_6]^{2-}$ were analyzed in greater depth. To facilitate comparisons, the Pd−Cl distance was fixed at the LDA-optimized value of 2.32 Å. Gradient corrections certainly reduce the binding energy and by some 362 kJ mol^{-1} for $[PdCl_6]^{2-}$. A Mulliken analysis of the charge distribution indicates that the BP description of the Pd−Cl bonding is more ionic in that the calculated Pd and Cl charges of 1.60 and −0.60 are closer to their formal values than the LDA charges of 1.37 and −0.56, respectively. The movement of charge is illustrated in Figure 5 where the difference between the total LDA and total BP densities is plotted. The negative contours around the edges of the Cl ions indicate greater charge in the BP density while the positive contours around the periphery of the metal are consistent with less electron density. These gross charge movements describe the dominant features in Figure 5, but closer to the metal, there is a separation of the bonding into its σ and π symmetry components. For a formally low-spin d^6 Pd^{4+} ion, the t_{2g} orbitals are filled while the e_g orbitals are empty. Charge donation from the Cl ligands will therefore lead to an increase of e_g density, and since the donation is reduced at the BP level, there will be more e_g density at the LDA level consistent with the positive σ symmetry contours in Figure 5. Given that the t_{2g} functions are formally filled at both levels of theory, the negative π symmetry features require a more subtle argument. The higher metal charge at the BP level should result in a general contraction of the electron density around the Pd centre. This concentration of charge would manifest as negative contours in Figure 5. The contraction/expansion of the density around nuclei as a function of the overall atomic charge tends to operate in the same sense as the gross charge movements described above at the edges of the atoms.

Ziegler's extended transition state (ETS) scheme[1a] can be used to separate the change in binding *energy* into its steric and orbital components (Table 4). The steric energy has two parts: the Pauli repulsion and the electrostatic interaction. The latter changes little from LDA to BP, while the Pauli repulsion is more positive by 226 kJ mol^{-1}. The total orbital interaction, which is less negative by about 100 kJ mol^{-1}, can also be factored by irreducible representation of the O_h point group. All the individual interactions decrease fairly uniformly, and given that we can loosely associate a_{1g}, e_g, t_{2g}, and t_{1u} symmetries with Pd−Cl interactions involving the metal s, d_σ, d_π, and p orbitals, respectively, this seems to suggest a relatively uniform reduction in Pd−Cl orbital interactions as already suggested by the charge density analysis. This should also tend to reduce the Pd−Cl contribution to the Pauli repulsion, but evidently, the greater density on and general expansion of the Cl ligands outweighs this and a large overall increase in steric repulsion results. The latter represents about two thirds of the change in total binding energy. Figure 6 shows the difference between the orthogonalized densities from LDA and BP calculations, *i.e.*, prior to orbital overlap. Relative to the LDA density, the BP calculation moves density from the periphery of the Pd atom and near the nuclei of the Cl atoms to the exterior of the Cl atoms and the interior of the Pd atom. These features are consistent with the Cl ligands expanding at the BP level while the Pd density contracts. In summary, the BP functional reduces the LDA overbinding by decreasing the covalency and giving generally more ionic bonding in these $[MX_6]^{2-}$ complexes. However, the more accurate BP estimates of the binding energies are not accompanied by better estimates of M−X distances. Apparently, the superior performance of the LDA for describing M−L distances in Werner complexes is fortuitous.

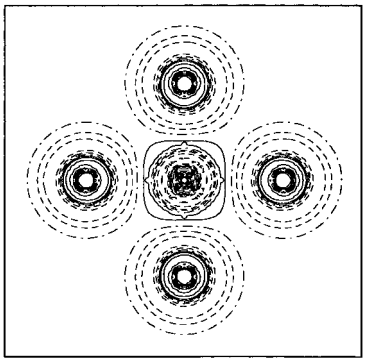

Figure 6. Calculated difference between total orthogonal electron densities (LDA-BP) in the *xy* plane of $[PdCl_6]^{2-}$. Solid contours represent positive values, dashed contours negative values, and the dot-dash contour is zero. The lowest contour level is ±0.000 23. Successive contours differ by a factor of 2.

Conclusions

Updated measures of the heterolytic M−X bond energies for a range of octahedral first-, second-, and third-row transition metal hexahalide complexes have been derived from experimental heats of formation and other thermodynamic data in conjunction with accurate theoretical lattice energies for antifluorite crystals of general formula A_2MX_6. These data are ideally suited for evaluating the relative performance of various DFT functionals with respect to the M−X binding energies in Werner-type metal complexes. As for other classes of chemical compound, the LDA overestimates the M−X bond energy, while the BP GC functional gives substantial improvements. Nevertheless, the BP-optimized *in vacuo* M−X distances are overall in poorer agreement with crystal structure data than the equivalent LDA results. Calculations on a model 'in crystal' $\{K_8[PdCl_6]\}^{6+}$ cluster suggest that the optimized bond lengths are not very sensitive to the crystalline environment, while calculations on *in vacuo* $[PdCl_6]^{2-}$ show that the heterolytic Pd-Cl bond energy is not very sensitive to the Pd−Cl distance. The LDA formally refers to a uniform or slowly varying density. The limit of purely ionic bonding corresponds to the greatest departure from a uniform electron gas and, presumably, to the worst case for the LDA. One can speculate that the LDA is somehow trying to force the density to be more uniform which then yields too much covalency and an overestimation of the binding energy. GC functionals can compensate to some extent and the resulting reduction in binding is accompanied by a lengthening of the M−L bonds. What still remains unclear is why the LDA gives good M−L distances in the first instance. The implications from this work and our previous study[3b] are

that the better M−L distances for Werner complexes obtained with the LDA are somehow fortuitous. However, we hope that these results may give some insights to guide the development of improved functionals which can simultaneously provide a more uniform treatment of both organometallic and Werner complexes.

References and Notes

(1) (a) Deeth, R. J. *Structure and Bonding*; **1995**, *82*, 1. (b) Ziegler, T. *Chem. Rev.* **1991**, *91*, 651. (c) Labanowski, J. K.; Andzelm, J. W. *Density Functional Methods in Chemistry*; Springer-Verlag: New York, 1991. (d) Bray, M. R.; Deeth, R. J. *Inorg. Chem.* **1996**, *35*, 5720. (e) Deeth, R. J.; Elding, L. I. *Inorg. Chem.* **1996**, *35*, 5019.

(2) Veillard, A. *Chem. Rev.* **1991**, *91*, 743.

(3) (a) Becke, A. D. *J. Chem. Phys.* **1992**, *96*, 2155. (b) Bray, M. R.; Deeth, R. J.; Paget, V. J.; Sheen, P. D. *Int. J. Quantum Chem.* **1997**, *61*, 85.

(4) (a) Becke, A. D. *Phys. Rev.* **1988**, *A38*, 3098. (b) Perdew, J. P. *Phys. Rev.* **1986**, *B33*, 8822. (c) Perdew, J. P. *Phys. Rev.* **1987**, *B34*, 7406.

(5) (a) Wang, Y.; Perdew, J. P. *Phys. Rev.* **1991**, *B43*, 8911. (b) Perdew, J. P. *Physica* **1991**, *B172*, 1.

(6) Since the thermochemistry and metal−ligand bond energies were published in 1979, the values of key thermodynamic quantities have undergone considerable revision, therefore necessitating the recomputation of the values. For example: $\Delta_f H^o(K^+,g) = 514.26$ kJ mol^{-1}, $\Delta_f H^o(Rb^+,g) = 490.101$ kJ mol^{-1}, $\Delta_f H^o(Cs^+,g) = 457.964$ kJ mol^{-1}, $\Delta_f H^o(F^-,g) = -255.39$ kJ mol^{-1}, $\Delta_f H^o(Cl^-,g) = -233.13$ kJ mol^{-1}, and $\Delta_f H^o(Br^-,g) = -219.07$ kJ mol^{-1} are the currently accepted thermodynamic values which differ individually by as much as 15 kJ mol^{-1} compared to the values used in 1979 (eqs 57−64 of ref 7a) to calculate the original bond energies.

(7) (a) Jenkins, H. D. B.; Pratt, K. F. *Adv. Inorg. Chem. Radiochem.* **1979**, *22*, 1. (b) Jenkins, H. D. B.; Pratt, K. F. *Prog. Solid State Chem.* **1979**, *12*, 125. (c) Blandamer, M. J.; Burgess, J.; Hamshere, S. J.; Peacock, R. D.; Rogers, J. H.; Jenkins, H. D. B. *J. Chem. Soc., Dalton Trans.* **1981**, 726.

(8) (a) Jenkins, H. D. B.; Pratt, K. F. *Proc. Roy. Soc. London* **1977**, *A356*, 115. (b) Jenkins, H. D. B.; Pratt, K. F. *Comput. Phys. Commun.* **1978**, *5*, 341. (c) Jenkins, H. D. B.; Pratt, K. F. *J. Chem. Soc., Faraday Trans. 2* **1978**, *74*, 968. (d) Pratt, K. F. Ph.D. Thesis, University of Warwick, Coventry, 1978.

(9) (a) Jenkins, H. D. B.; Sharman, L.; Finch, A.; Gates, P. N. *Inorg. Chem.* **1996**, *35*, 6316. (b) Jenkins, H. D. B. *Polyhedron* **1996**, *15*, 2831.

(10) Basolo, F.; Pearson, R. G. *Mechanisms of Inorganic Reactions*; Wiley: New York, 1958.

(11) Jenkins, H. D. B. In *Handbook of Chemistry and Physics*, 6th ed.; Lide, D. R., Ed.; CRC Press: Boca Raton, 1995−1996.

(12) Wagman, D. D.; Evans, W. H.; Parker, V. B.; Schumm, R. H.; Halow, I.; Bailey, S. M.; Churney, K. L.; Nuttall, R. L. NBS Tables of Chemical Thermodynamic Properties. *J. Phys. Chem. Ref. Data* **1982**, *11* (Suppl. 2).

(13) (a) Hopkins, K. G. G. Ph.D. Thesis, University of Hull, 1970. (b) Moore, C. E. *Analysis of Optical Spectra*; NSRDS-NBS34; Office of Reference Data, National Bureau of Standards, U.S. Government Printing Office: Washington, DC, 1958. (c) Moore, C. E. *Ionisation Potentials and Ionisation Limits Derived from the Analysis of Optical Spectra*; National Standard Reference Data Series 34; National Bureau of Standards, U.S. Government Printing Office: Washington, DC, 1970. (d) Sugar, J.; Corliss, C. Atomic Energy Levels of Iron Period Elements: Potassium through Nickel. *J. Phys. Chem. Ref. Data* **1985**, *14* (Suppl. 2). (e) Lide, D. R. *Handbook of Chemistry and Physics*; 76th ed.; Lide, D. R., Ed.; CRC Press: Boca Raton, 1995−1996. (f) Efimov, A. I.; Belorukova, L. P. *Russ. J. Inorg. Chem.* (*Transl. of Zh. Neorg. Khim.*) **1967**, *12*, 792. (g) Pedley, J. D. *CATCH Thermochemical Tables*; University of Sussex, 1974. (h) Korol'kov, D. V.; Efimov, A. I. *Probl. Sovrem. Khim. Koord. Soedin.* **1966**, *1*, 215. (i) Rossini, F. D.; Wagman, D. D.; Evans, W. H.; Levine, S.; Jaffe, I. *Natl. Bur. Stand. Circ* (*U.S.*) **1952**, *500*. (j) Welsh, W. A.; Brill, T. B.; Thompson, P. T.; Wood, R. H.; Gearhart, R. C. *Inorg. Chem.* **1974**, *13*, 1797. (k) Shchukarev, S. A.; Vasil'kova, C. V.; Korol'kov, D. V. *Russ. J. Inorg. Chem.* (*Transl. of Zh. Neorg. Khim*). **1964**, *9*, 980. (l) Gelbman, P.; Westland, A. D. *J. Chem. Soc., Dalton Trans.* **1974**, 1598. (m) Peacock, R. D. Private Communication. (n) Korol'kov, D. V.; Efimov, A. I. *Russ. J. Inorg. Chem. (Transl. of Zh. Neorg. Khim.)* **1970**, *15*, 1759. (o) Parker, V. B.; Wagman, D. D.; Evans, W. H. *NBS Tech. Note.* (*U.S.*) **1971**, *270*. (p) Busey, R. H.; Gayer, K. H.; Gilbert, R. A.; Bevan, R. B. *J. Phys. Chem.* **1966**, *70*, 2609. (q) Blandamer, M. J.; Burgess, J.; Hamshere, S. J.; Peacock, R. D.; Rogers, J. H.; Jenkins, H. D. B. *J. Chem. Soc., Dalton Trans.* **1981**, 726. (r) Wagman, D. D.; Evans, W. H.; Parker, V. B.; Schumm, R. H. *Chemical Thermodynamic Properties of Sodium, Potassium and Rubidium: An Interim Tabulation of Selected Values*; NBSIR 76-1034; Office of Standard Reference Data, National Bureau of Standards, U.S. Government Printing Office; Washington, DC, 1973. (s) Burgess, J.; Cartwright, S. J. *J. Chem. Soc., Dalton Trans.* **1975**, *100*. (t) Goldberg, R. N.; Hepler, L. G. *Chem. Rev.* **1968**, *68*, 229. (u) Bamburov, V. G. *Trudy Inst. Khim. Uralskogo. Felialia AN SSSR* **1963**, *7*, 27. (v) Shidlovskii, A. A. *Zh. Fiz. Khim.* **1964**, *B19*, 1237. (w) Shchkarev, S. A.; Vasil'kova, C. V.; Korol'kov, D. V. *Russ. J. Inorg. Chem.* **1964**, *9*, 980.

(14) Kohn, W.; Sham, L. J. *Phys. Rev.* **1956**, *140*, A1133.

(15) (a) Baerends, E. J.; Ellis, D. E.; Ros, P. *Chem. Phys.* **1973**, *2*, 41. (b) te Velde, B.; Baerends, E. J. *Int. J. Quantum Chem.* **1988**, *33*, 87.

(16) Vosko, S. H.; Wilk, L.; Nusair, M. *Can. J. Phys.* **1980**, *58*, 1200.

(17) Versluis, L.; Ziegler, T. *J. Chem. Phys.* **1988**, *88*, 322.

(18) Snijders, J. G.; Baerends, E. J. *Mol. Phys.* **1978**, *36*, 1789. (b) Snijders, J. G.; Baerends, E. J.; Ros, P. *Mol. Phys.* **1979**, *38*, 1909.